

AAAAAAA

A DISSERTATION PRESENTED
BY
FRANCESCO IOLI
TO
THE DEPARTMENT OF PSYCHOLOGY

IN PARTIAL FULFILLMENT OF THE REQUIREMENTS
FOR THE DEGREE OF
DOCTOR OF PHILOSOPHY
IN THE SUBJECT OF
PSYCHOLOGY

HARVARD UNIVERSITY
CAMBRIDGE, MASSACHUSETTS
MAY 2024

©2023 – FRANCESCO IOLI
ALL RIGHTS RESERVED.

AAAAAAA

ABSTRACT

Lorem ipsum dolor sit amet, consectetuer adipiscing elit. Morbi commodo, ipsum sed pharetra gravida, orci magna rhoncus neque, id pulvinar odio lorem non turpis. Nullam sit amet enim. Suspendisse id velit vitae ligula volutpat condimentum. Aliquam erat volutpat. Sed quis velit. Nulla facilisi. Nulla libero. Vivamus pharetra posuere sapien. Nam consectetuer. Sed aliquam, nunc eget euismod ullamcorper, lectus nunc ullamcorper orci, fermentum bibendum enim nibh eget ipsum. Donec porttitor ligula eu dolor. Maecenas vitae nulla consequat libero cursus venenatis. Nam magna enim, accumsan eu, blandit sed, blandit a, eros.

Quisque facilisis erat a dui. Nam malesuada ornare dolor. Cras gravida, diam sit amet rhoncus ornare, erat elit consectetuer erat, id egestas pede nibh eget odio. Proin tincidunt, velit vel porta elementum, magna diam molestie sapien, non aliquet massa pede eu diam. Aliquam iaculis. Fusce et ipsum et nulla tristique facilisis. Donec eget sem sit amet ligula viverra gravida. Etiam vehicula urna vel turpis. Suspendisse sagittis ante a urna. Morbi a est quis orci consequat rutrum. Nullam egestas feugiat felis. Integer adipiscing semper ligula. Nunc molestie, nisl sit amet cursus convallis, sapien lectus pretium metus, vitae pretium enim wisi id lectus. Donec vestibulum. Etiam vel nibh. Nulla facilisi. Mauris pharetra. Donec augue. Fusce ultrices, neque id dignissim ultrices, tellus mauris dictum elit, vel lacinia enim metus eu nunc.

Contents

Listing of figures

Acknowledgments

LOREM IPSUM DOLOR SIT AMET, consectetur adipiscing elit. Morbi commodo, ipsum sed pharetra gravida, orci magna rhoncus neque, id pulvinar odio lorem non turpis. Nullam sit amet enim. Suspendisse id velit vitae ligula volutpat condimentum. Aliquam erat volutpat. Sed quis velit. Nulla facilisi. Nulla libero. Vivamus pharetra posuere sapien. Nam consectetur. Sed aliquam, nunc eget euismod ullamcorper, lectus nunc ullamcorper orci, fermentum bibendum enim nibh eget ipsum. Donec porttitor ligula eu dolor. Maecenas vitae nulla consequat libero cursus venenatis. Nam magna enim, accumsan eu, blandit sed, blandit a, eros.

1

Introduction

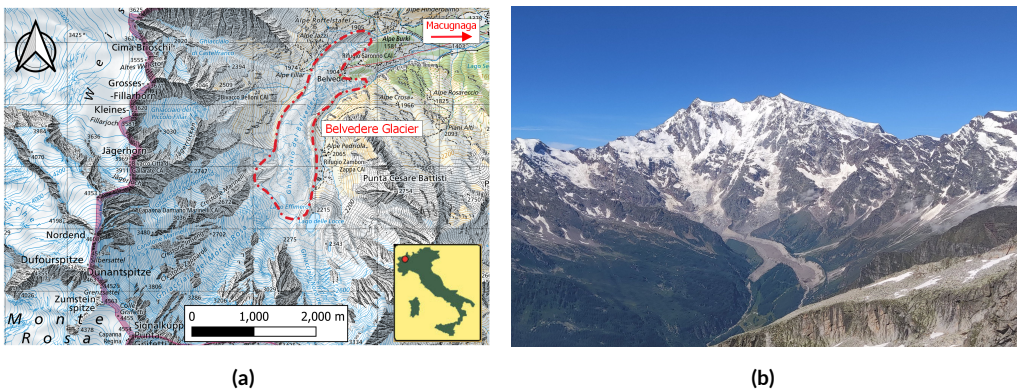


Figure 1.1: (a) Location of Belvedere Glacier, base map (source: Swisstopo www.geo.admin.ch); (b) Picture of ...

1.1 MOTIVATION AND RELEVANCE

1.2 THE BELVEDERE GLACIER

The Belvedere Glacier (Randolph Glacier Inventory code RGI60-11.02858) is an alpine glacier in Valle Anzasca (Italy), on the east side of the Monte Rosa Massif ($N\ 45^{\circ}58' E\ 7^{\circ}55'$) (Fig. ??). The lower part of the Belvedere Glacier is a temperate debris-covered glacier, that covers an area of $\sim 1.8\ km^2$ and extends from an altitude of $\sim 2250\ m\ a.s.l.$ to $\sim 1800\ m\ a.s.l.$. This region is characterized by a gentle slope, and it is fed by ice falls and snow avalanches coming from the Monte Rosa East Face (?). In its low-relief sector, the Belvedere Glacier splits into two lobes, reaching $\sim 1800\ m\ a.s.l.$. The northern lobe, in particular, ends with a prominent ice cliff, from which the River Anza springs.

Similarly to Miage glacier (Monte Bianco, Valle d'Aosta), the Belvedere Glacier is almost completely covered by rocks and boulders with dimensions ranging from few decimetres to some meters, which makes it a *black glacier*. Due to the global warming trend, the number of black glaciers along the Italian Alps is rising (?). Up to the beginning of the century, the debris cover helped to compensate the effect of the increased temperature, establishing a negative feedback in the temperature-ablation relationship (??). However, in recent years, the debris cover protection has not been sufficient to limit the glacier retreat.

In the past, several hazardous events originated by the Belvedere Glacier, such as floods and slope instability, threatened the nearby village of Macugnaga and the Zamboni Zappa Hut, at $2070\ m\ a.s.l.$ (?). At the beginning of the 21st century, the Belvedere Glacier was characterized by a particular surge-type dynamics (?). During the late 1990s, the surface speeds of the whole glacier were ranging between $30\ m\ y^{-1}$ and $45\ m\ y^{-1}$ (??). During 2000–2001 an accelerated flow in the Monte-Rosa Glacier produced a wave of compression-decompression stresses and strains in the Belvedere Glacier. Surface velocities soared: values up to $200\ m\ y^{-1}$ were observed photogrammetrically during autumn 2001 (?). The ice thickness increased more than $20\ m$ and the wave travelled downwards, creating a depression area in the accumulation zone, that was filled by a super-glacial lake, the Lago Effimero (??).

I.3

I.4

References

- Diolaiuti, G., D'Agata, C., & Smiraglia, C. (2003). Belvedere Glacier, Monte Rosa, Italian Alps: Tongue Thickness and Volume Variations in the Second Half of the 20th Century. *Arctic, Antarctic, and Alpine Research*, 35(2), 255–263.
- Haeberli, W., Kääb, A., Paul, F., Chiarle, M., Mortara, G., Mazza, A., Deline, P., & Richardson, S. (2002). A surge-type movement at Ghiacciaio del Belvedere and a developing slope instability in the east face of Monte Rosa, Macugnaga, Italian Alps. *Norsk Geografisk Tidsskrift*, 56(2), 104–111.
- Kääb, A., Huggel, C., Barbero, S., Chiarle, M., Cordola, M., Epifani, F., & Haeberli, W. (2004). Glacier Hazards At Belvedere Glacier and the Monte Rosa East Face , Italian Alps: Processes and Mitigation. *Inter nationales Symposion INTERPRAEVENT 2004 – RIVA / TRIENT*, (Vc), 67–78.
- Kääb, A., Huggel, C., Fischer, L., Guex, S., Paul, F., Roer, I., Salzmann, N., Schlaefli, S., Schmutz, K., Schneider, D., Strozzi, T., & Weidmann, Y. (2005). Remote sensing of glacier-and permafrost-related hazards in high mountains: an overview. *Natural Hazards and Earth System Science*, 5(4), 527–554.
- Mortara, G., Tamburini, A., Ercole, G., Semino, P., Chiarle, M., Godone, F., Giuliano, M., Haeberli, W., Kääb, A., Huggel, C., Fischer, L., Cordola, M., Barbero, S., Salandin, A., Rabuffetti, D., Mercalli, L., Berro, D. C., Carton, A., Mazza, A., Godone, D., Federici, P., Viazzi, G., Epifani, F., & Valsesia, T. (2009). *Il ghiacciaio del Belvedere e l'emergenza del Lago Effimero. Regione Piemonte*. Societa' Meteorologica Subalpina.
- Roethlisberger, H., Haeberli, W., Schmid, W., Biolzi, M., & Pika, J. (1985). Studi Sul Comportamento Del Ghiacciaio Del Belvedere. *Comunità montana della Valle Anzasca*, (97.3).

2

Background

References

3

UAV photogrammetry for...

THIS CHAPTER IS BASED ON:

Ioli, F., Bianchi, A., Cina, A., De Michele, C., Maschio, P., Passoni, D., & Pinto, L. (2021). Mid-Term Monitoring of Glacier's Variations with UAVs: The Example of the Belvedere Glacier. *Remote Sensing*, 14(1), 28. <https://doi.org/10.3390/rs14010028>

3.1 INTRODUCTION

3.2 INSTRUMENTS AND DATASETS

Short intro to section...

3.2.1 UAV FLIGHTS

Because of the long duration of the monitoring campaign, the challenging environment and the fact that more than one research group was involved in the project, different UAV platforms and cameras were used. As reported in Table ??, in 2015 and 2016, a ready-to-fly fixed-wing UAV SenseFly eBee, equipped with a compact camera Canon PowerShot S110, was employed to survey the whole glacier. During 2017, different combinations of UAVs (fixed-wing and quadcopters) and cameras were employed (Table ??). From 2018 to 2020, a low-cost recreational fixed-wing UAV Parrot Disco FPV, with a wingspan of 1.15 m and a weight of 750 g, was adapted to carry a small and lightweight action cam Hawkeye Firefly 8S. For each camera, the main sensor and objective characteristics are listed Table ??.

UAVs flights were conducted automatically by using ground station software packages developed by UAV manufacturers. Add UGCS...

The flights were designed to have GSD ranging between 5 cm and 10 cm, and to guarantee $\sim 80\%$ of longitudinal and $\sim 60\%$ of transversal overlap. Average image GSD values and number of GCPs and CPs, used respectively to orient the images and to assess the quality of the photogrammetric blocks, are summarized in Table ??.

Add instruments for 2021-2023...

3.2.2 GNSS MEASUREMENTS

A set of GCPs was materialized with square cross targets, printed on polypropylene sheets and anchored on big rocks (Figure ??b). About 25 targets were deployed over the glacier (named hereafter as *moving targets* or *M#* in Figure ??a) and 24 targets (labelled as *stable targets* or *S#* in Figure ??a) were placed on stable areas along the moraines so that they were not subjected neither to the ice flow nor to rock falls. Every year, the condition of each target was checked and, if one was damaged or destroyed, the polypropylene sheet was replaced by keeping the same location of the center (i.e., by using the same fisher plugs). During the years, some targets were lost, and therefore new ones were materialized (e.g., M29bis). Targets were yearly surveyed with dual frequency (L1/L2) geodetic quality GNSS receivers and their coordinates were framed within the official Italian reference system ETRF2000 at the epoch 2008.0, projected in UTM 32N. For the lower part of the glacier, where the GSM network connection was available, target position was obtained in nRTK with respect to a network of CORS permanent stations (either HxGN SmartNet or SPIN GNSS). The points were occupied at least twice, each time for a duration of 5 s. By contrast, in the upper part of the glacier, targets were surveyed with static sessions of ~ 10 min, and raw observation data was post-processed with respect to local master

Table 3.1: Summary of the characteristics of the surveys.

Year	Date	UAV	Camera	GSD [m/px]	GCP [#]	CP [#]
2015	A. 8.10 B. 23.10	SenseFly eBee	Canon PowerShot S110	0.07	24	11
2016	20.10	SenseFly eBee	Canon PowerShot S110	0.09	31	15
2017	A. 5.10 B. 15.11 C. 16.11	A. SenseFly eBee B. SenseFly eBee Plus C. DJI Phantom 4 Pro	A. Canon PowerShot S110 B. SenseFly S.O.D.A C. DJI FC6310	0.06	27	8
2018	23-25.07	Parrot Disco	Hawkeye Firefly 8S	0.05	27	13
2019	29.07- 2.08	Parrot Disco	Hawkeye Firefly 8S	0.06	26	10
2020	A. 26- 27.07 B. 9.08	A. Parrot Disco B. DJI Phantom 4 Pro	A. Hawkeye Firefly 8S B. DJI FC6310	0.05	29	12

Table 3.2: Summary of the characteristics of the cameras employed.

Camera	Sensor	Sensor Size [mm ²]	Focal length [mm]	Image size [px]	Pixel size [μm]
Canon PowerShot S110	1/1.7" CMOS	7.44 × 5.58	5.2	4000 × 3000	1.9
SenseFly S.O.D.A	1" CCD	13.2 × 8.8	10.6	5472 × 3648	2.4
DJI FC6310	1" CMOS	13.2 × 8.8	8.8	5472 × 3648	2.4
Hawkeye Firefly 8S	1/2.3" CMOS	6.17 × 4.56	3.8	5472 × 3648	1.34

stations, located on stable and well known points. To this end, either the point S_{12} , placed on a big rock next to the Zamboni-Zappa hut, or the point S_{20} , located near the Rifugio Ghiacciai del Rosa on the Belvedere hill, were used (see Figure ??a). Accuracy of GNSS measurements was evaluated empirically by comparing repeated measurements over stable targets carried out in different years. RMSE of 1.5 cm in planimetry and 3 cm in elevation were obtained.

3.3 METODOLOGY

3.3.1 SfM WORKFLOW

In order to build photogrammetric models of the glacier, images acquired during UAV surveys were processed with the SfM software Agisoft Metashape 1.7.2 (?). For each year, at least 24 GCPs spread over the glacier were employed to orient the images, whereas at least 10 Check Points (CPs) were used to assess models quality. Both GCPs and CPs were manually collimated on the images. Tie Points (TPs) were detected and matched by Metashape on full resolution images (which corresponds to *high accuracy* parameter in Metashape). Image External Orientation (EO) and TPs world coordinates were estimated by solving the Bundle Block Adjustment (BBA). TPs with the worst reprojection error on images, which are likely originated from false matches, were removed and the BBA was solved again to improve quality of BBA solution. This process was iterated more times until TPs mean reprojection error had dropped below 0.7-0.8 px. Camera internal orientation was estimated by self-calibration (??), because of its instability in the cameras employed.

Dense 3D reconstruction was computed by Agisoft Metashape with proprietary MVS algorithms (?). Depth maps and dense point clouds were obtained from images downsampled by a factor 4, in order to reduce the computational time (*medium quality* parameter of the dense cloud generation in Metashape). Triangulated mesh surfaces and photorealistic textures were computed.

DSMs with a resolution of 0.5 m px^{-1} were derived from the mesh model. Finally, orthophotos with a GSD of 0.10 m px^{-1} were obtained by projecting the most nadiral images over the mesh model (Figure ??).

3.3.2 GLACIER FLOW VELOCITY

3.3.3 VOLUME VARIATIONS

To compute glacier volume variation ΔV , consecutive DSMs were differentiated by employing a DEM of Difference (DOD) approach with the tool *Compute 2.5 D volume* implemented in CloudCompare ?. First, photogrammetric dense clouds were gridded by projecting points along the vertical direction on a planar surface, obtaining DSMs with a cell footprint on ground of $0.5 \text{ m} \times 0.5 \text{ m}$. The choice of the raster resolution was a compromise to achieve a robust height field estimation by averaging a large enough number of points for each cell of the raster, but at the same time small enough to maintain a spatial resolution able to map small scale glacier morphology. A mask was manually created and

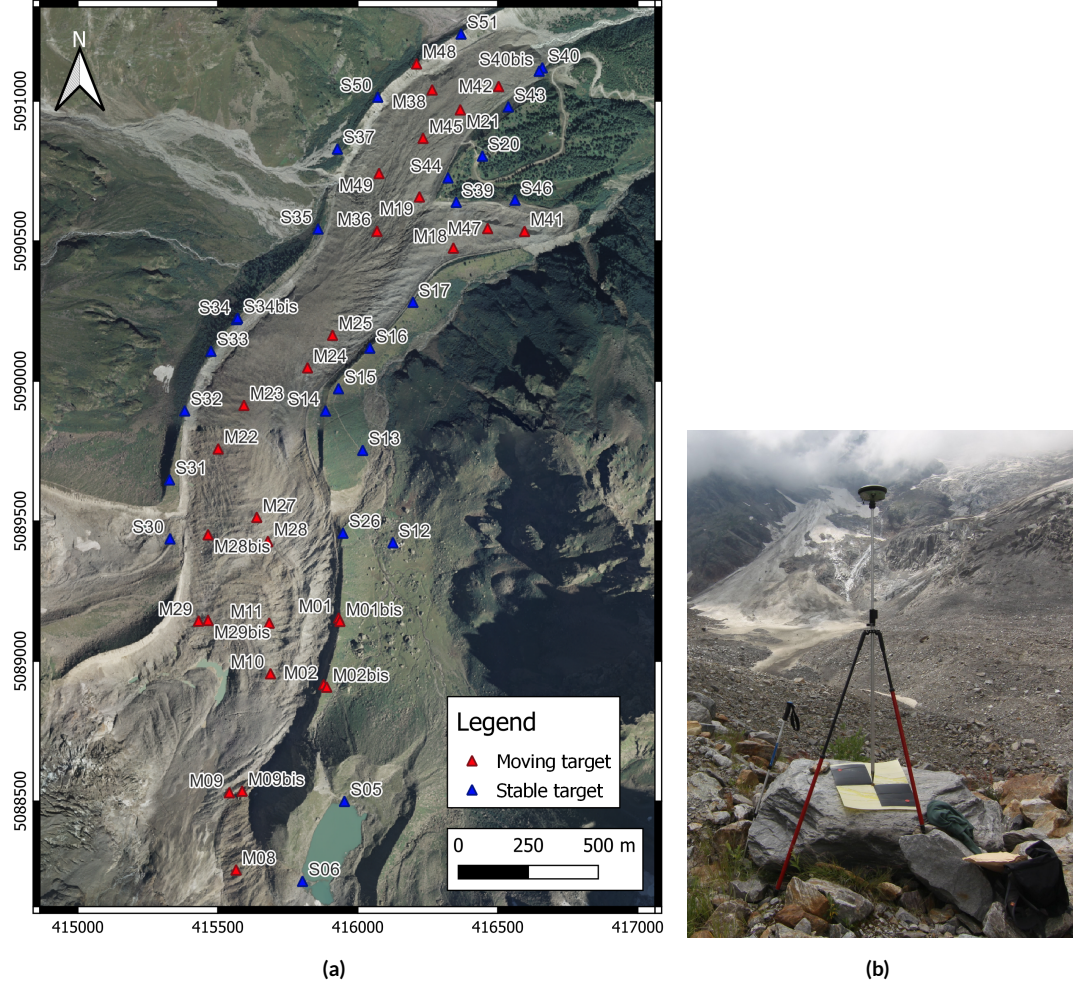


Figure 3.1: (a) An example of a photogrammetric target deployed over the glacier moraine; (b) location of the targets used for the photogrammetric surveys. For each year, a subset of the targets were used as GCPs, while the remaining as CPs.

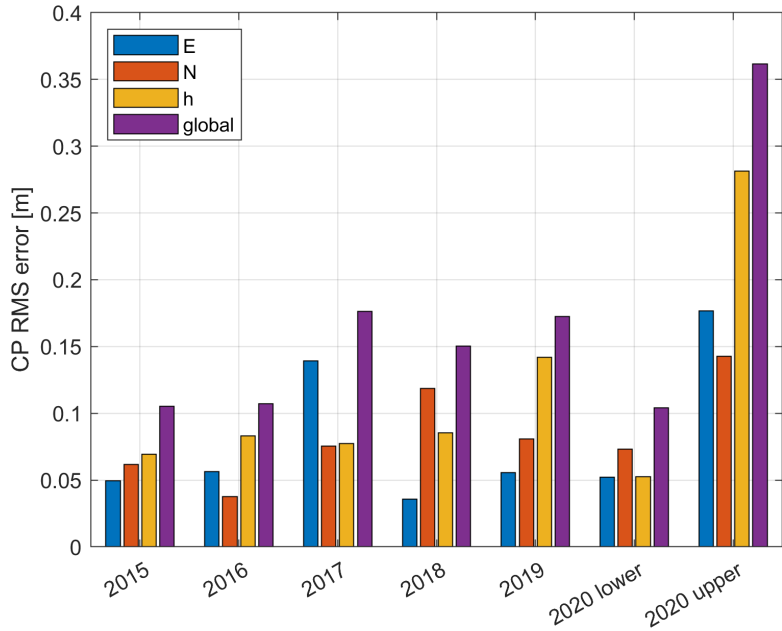


Figure 3.2: Barplot of reprojection RMSE computed CPs for each photogrammetric model. Due to practical problems occurred in 2020 and explained in Section ??, the RMSE of 2020 model was split in two parts: 2020 *lower* denotes the CP RMSE over related to the central and lower sectors of the glacier (S2 and S3 in Figure ??a), whereas 2020 *upper* refers to the upper accumulation sector only (S1).

applied to all the DSMs to exclude areas outside the glacier surface. DSMs from consecutive years were then differentiated pixel-by-pixel to obtain the height difference at each cell of the raster.

3.4 RESULTS

3.4.1 SFM

The re-projection RMSE over the CPs are shown in Figure ?? as assessment of the geometrical accuracy of the models. The global re-projection RMSE was mostly ranging between 0.1 m and 0.2 m. The only exception consisted in the upper sector (comparable to sector S1 in Figure ??a) of the 2020 model, for which the RMSE is almost double compared to the other values. This was caused by practical problems occurred in 2020, explained in detail in Section ???. As a consequence, the value of 2020 RMSE was split in two different bars in the graph. From 2015 to 2017, when compact cameras were used, errors comparable to 1.5 times the GSD were obtained. Since 2018, a lightweight action-cam has been employed to minimize the UAV take-off weight and this has led to an RMSE up to 3 times the GSD, but still always smaller than 0.2 m.

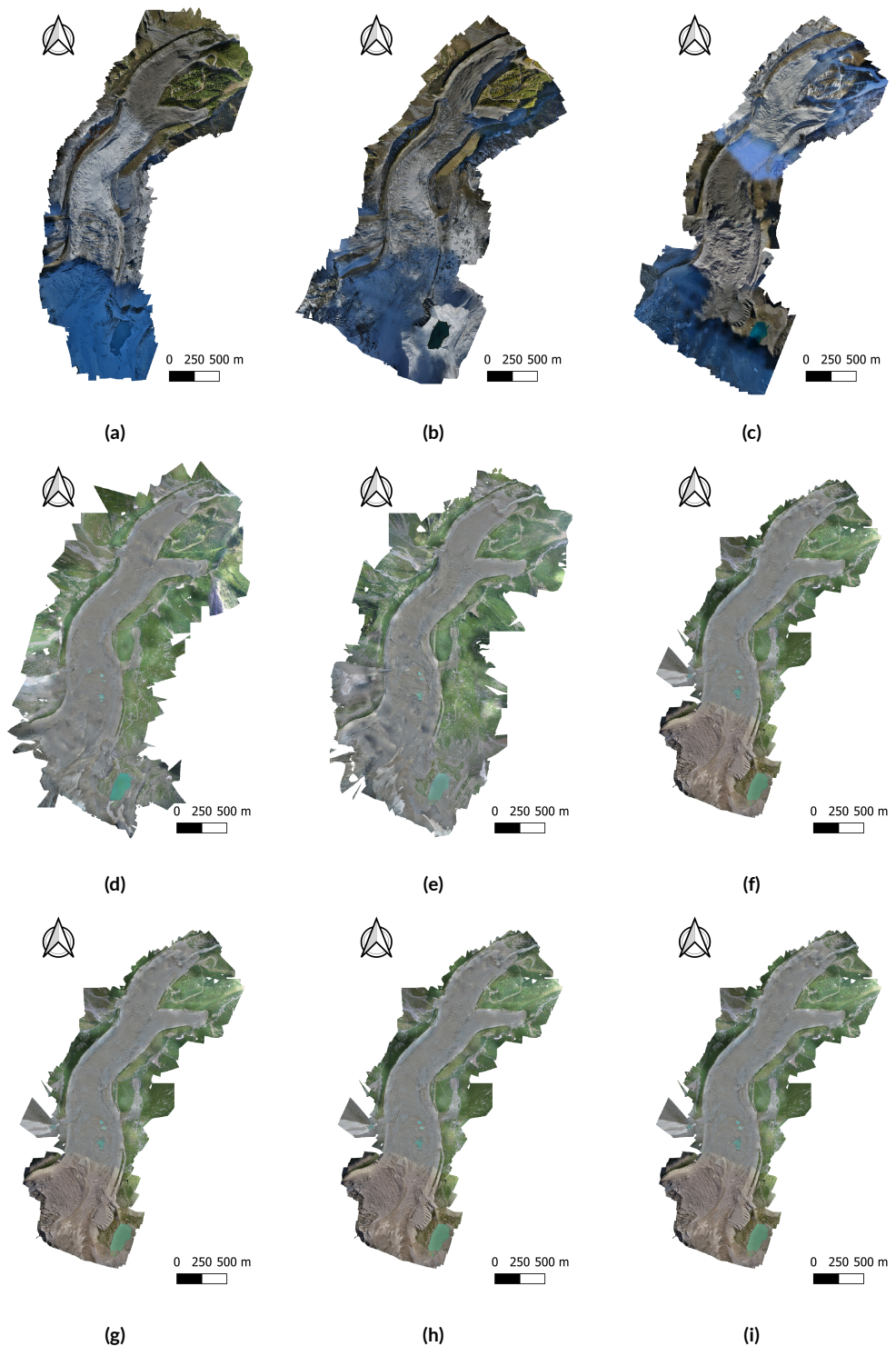


Figure 3.3: Orthophotos obtained from the photogrammetric model for each year. (a) 2015, (b) 2016, (c) 2017, (d) 2018, (e) 2019, (f) 2020, (g) 2021, (h) 2022, (i) 2023.

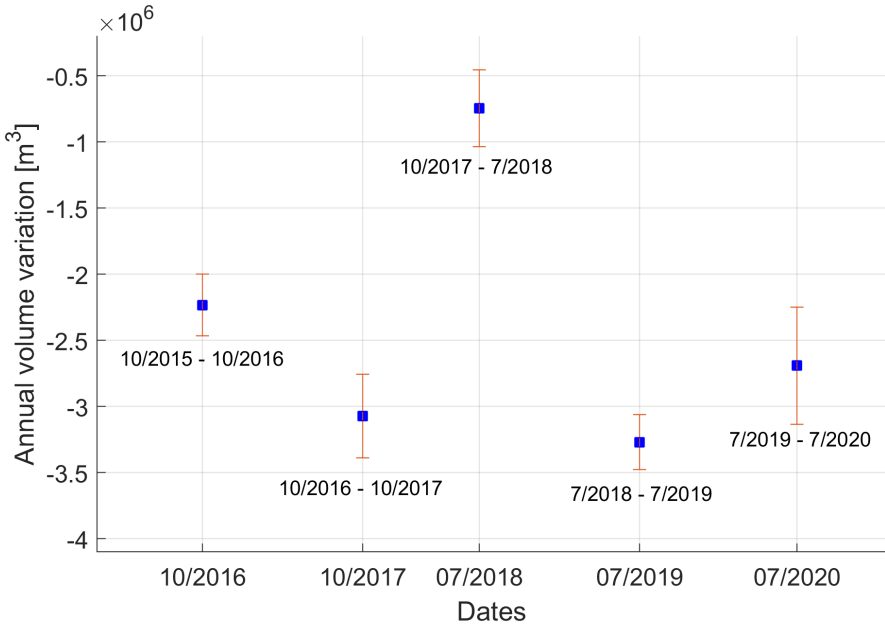


Figure 3.4: Yearly volume variation computed as difference between DSM of two consecutive years. The error bars plotted represent the uncertainty of each estimated value. Note that the values on the Y axis are expressed in million of m³.

3.4.2 GLACIER FLOW VELOCITY

3.4.3 VOLUME VARIATIONS

Add 2021-2023!

In order to rigorously estimate volume variation variances, by propagating the variance, it would be necessary to know the covariance matrix of each DSM, considered as a multivariate random variable with dimension equal to the number of cells. However, no information concerning cells covariances was provided by the SfM software employed, thus it was troublesome to compute covariances between nearby cells in a DSM (which are clearly correlated because they were generated by the same set of images in the photogrammetric process). As a consequence, only a rough estimation of the variance was carried out by considering each DSM as a mono-dimensional random variable with variance equal to the squared value of the vertical component of RMSE computed on the CPs of the relative photogrammetric model (see Figure ??). Moreover, $DSM^{(i+1)}$ and $DSM^{(i)}$ were considered as independent because there was no relation between the surveys. The variance of the volume variation was therefore computed as:

$$\sigma_{\Delta V^{(i+1,i)}}^2 = (n \times A_c)^2 (\sigma_{DSM^{(i+1)}}^2 + \sigma_{DSM^{(i)}}^2), \quad (3.1)$$

where n is the number of cell in the DSMs and σ_{DSM}^2 is the squared vertical error of the photogrammetric model evaluated on the GCPs.

For the years 2015–2016, 2016–2017, 2017–2018, the glacier was partially covered by snow (see Figure ??a–c), which introduced additional uncertainties in volume estimation. The snow height accumulated at the nivometric station located near Zamboni Zappa Hut (2075 m a.s.l., in the central sector of the glacier) on the survey dates was retrieved from the meteorological database of ARPA Piemonte, the regional agency for the environment ?: 22 cm of snow were measured on 23 October 2015, 20 cm on 20 October 2016, 40 cm on 15 November 2017. The measured snow heights were considered as additional components of DSM standard deviations. Yet, because the glacier was only partially covered by snow, the snow-driven uncertainty was weighted by half of the total glacier area in variance propagation. Figure ?? illustrates the loss of ice volume year by year. The estimated variance of the glacier volume variation is plotted as an error bar for each value of volume variation.

Between 2017 and 2018, fieldworks were moved from Autumn to Summer. Therefore, the loss of volume for the year 2017–2018 was computed between October 2017 and July 2018, therefore it represented only the variation occurred in wintertime and springtime, and it should not be directly compared with the annual average. Indeed, 2017–2018 volume variation was $-0.75 \times 10^6 \text{ m}^3$, against the average variation between 2015 and 2020 of $-2.81 \times 10^6 \text{ m}^3$ (difference of 27 %). Ice volume loss for the year 2019–2020 may be slightly underestimated as well: the photogrammetric model of the upper part of the glacier was affected by a larger geometric (RMSE in vertical direction of = 0.28 m, see Section ??) compared to the others models, due to the lack of GCPs measured in-situ at the time of the photo acquisition. Overall, the negative ice volume variation occurred between 2015 and 2020 is evident and significant: every year, between $2 \times 10^6 \text{ m}^3$ and $3.5 \times 10^6 \text{ m}^3$ of ice were lost.

3.4.4 GLACIER OUTLINE

3.4.5 PROBLEMS ARISING DURING THE SURVEYS OF 2017 AND 2020

Conducting a yearly monitoring campaign in an alpine environment for six consecutive years is challenging because of, for example, the hard accessibility of some areas of the glacier (also for fixed-wing UAVs take-off and landing) and the variability of the meteorological conditions.

Adverse meteorological conditions and practical issues made it necessary to split the 2017 survey in different dates, and various UAVs and cameras were employed (see Table ??). The 2017 photogrammetric model was therefore divided into three parts: the central part refers to the October survey while the lower and the upper parts refer to the November survey and at that time the glacier was covered by snow (Figure ??c). Technical problems arose also during the 2020 survey: a breakage of one elevon servo during a landing phase caused the fixed-wing UAV to crash. Therefore, a quadcopter DJI Phantom 4 Pro was employed to survey the upper part of the glacier (approximately the S1 sector, see the different colors in the orthophoto of Figure ??f) 14 days after the former. However, during the August 2020 fieldwork, it was not possible to measure any additional GCPs because the south-west part of the Belvedere Glacier, close to the Monte-Rosa Glacier is hardly accessible and dangerous due to the presence of crevasses and steep rocks. The few GCPs available in the upper part of the glacier made necessary to co-register the Phantom 4 Pro model on the 2019 model, by searching for sharp edges of rocks along the moraines, remained fixed along the year, on 2019 images. This approach is less accu-

rate than measuring targets directly on the field. The RMSE on CPs was therefore equal to 0.36 m (see Figure ??), ~ 7 times the GSD. Nevertheless, the area affected by this issue was rather limited, compared to the whole Belvedere Glacier.

Moreover, between 2017 and 2018, the survey period was moved from Autumn to Summer. From 2015 to 2017, in fact, fieldworks were included within the DREAM project (see Section ??) and they took place in Autumn, at the beginning of the academic year. By contrast, from 2018 to 2020, surveys were carried out at the end of July because they were encompassed within a Summer School organized by DICA (Politecnico di Milano). The change in the survey dates was critical because the timespan occurred between the survey of October/November 2017 and that of July 2018 did not include the period of maximum ablation and velocity of the glacier (neither August 2017 nor August 2018). Therefore, volume variation and ice flow velocity refer mostly the wintertime and the results obtained are not directly comparable with those of the other years.

3.5 DISCUSSION

Several studies focused on understanding and quantifying Belvedere Glacier dynamics. ? estimated velocities ranging between 32 m y^{-1} and 43 m y^{-1} on the whole Belvedere Glacier from October 1995 to September 1999, by employing aerial images. Besides, velocities between 100 m y^{-1} and 200 m y^{-1} were estimated by ? in Autumn 2001, during the extraordinary surge event of 2000–2001. Nowadays, the Belvedere Glacier is clearly moving slower compared to the late 1990s. However, to the best of authors knowledge, there are no recent works estimating glacier flow velocities.

Concerning volume variations, ? digitalized two large-scale topographic maps to interpolate DSMs and estimate volume variations between 1957 and 1991. They found a positive volume difference of $+22.7 \times 10^6 \text{ m}^3$ (with an average rate of $\sim 0.69 \times 10^6 \text{ m}^3 \text{ y}^{-1}$, roughly assuming a linear volume variation during the years). Their result matched with the study of ?, who estimated an increase of the glacier height of $+1.5 \text{ m y}^{-1}$ between 1983 and 1985. Recently, ? used historical aerial images and UAVs to photogrammetrically reconstruct glacier volume variations between 1977 and 2019. For the period 1977–1991, they confirmed the glacier expansion, with a volume increase of $+10.06 \times 10^6 \text{ m}^3$ ($+0.72 \times 10^6 \text{ m}^3 \text{ y}^{-1}$). The expansion continued up to 2001 (at the end of the surge event), with additional $10.61 \times 10^6 \text{ m}^3$ of ice gained. Since 2001, a severe glacier retreat has begun, with a loss of ice volume of $-47.78 \times 10^6 \text{ m}^3$ ($-5.97 \times 10^6 \text{ m}^3 \text{ y}^{-1}$) between 2001 and 2009. For the time-span 2009–2019, ? derived a negative variation of $-27.16 \times 10^6 \text{ m}^3$ of ice ($-2.72 \times 10^6 \text{ m}^3 \text{ y}^{-1}$). This last ten-years-averaged estimate well matches with the annual volume variations found in this study between 2015 and 2020 (between $-2 \times 10^6 \text{ m}^3 \text{ y}^{-1}$ and $-3.5 \times 10^6 \text{ m}^3 \text{ y}^{-1}$).

References

- Agisoft (2023). Metashape.
- De Gaetani, C. I., Ioli, F., & Pinto, L. (2021). Aerial and UAV Images for Photogrammetric Analysis of Belvedere Glacier Evolution in the Period 1977–2019. *Remote Sensing 2021, Vol. 13, Page 3787*, 13(18), 3787.
- Diolaiuti, G., D'Agata, C., & Smiraglia, C. (2003). Belvedere Glacier, Monte Rosa, Italian Alps: Tongue Thickness and Volume Variations in the Second Half of the 20th Century. *Arctic, Antarctic, and Alpine Research*, 35(2), 255–263.
- Kääb, A., Huggel, C., Fischer, L., Guex, S., Paul, F., Roer, I., Salzmann, N., Schlaefli, S., Schmutz, K., Schneider, D., Strozzi, T., & Weidmann, Y. (2005). Remote sensing of glacier-and permafrost-related hazards in high mountains: an overview. *Natural Hazards and Earth System Science*, 5(4), 527–554.
- Roethlisberger, H., Haeberli, W., Schmid, W., Biolzi, M., & Pika, J. (1985). Studi Sul Comportamento Del Ghiacciaio Del Belvedere. *Comunità montana della Valle Anzasca*, (97.3).

4

Back to the past: reconstructing glacier geometry with historical images (1977-2009)

THIS CHAPTER IS BASED ON:

De Gaetani, C. I., Ioli, F., & Pinto, L. (2021). Aerial and UAV Images for Photogrammetric Analysis of Belvedere Glacier Evolution in the Period 1977–2019. *Remote Sensing*, 13(18), 3787. <https://doi.org/10.3390/rs13183787>

4.1 INTRODUCTION

4.2 DATASETS

4.2.1 HISTORICAL AERIAL DATASETS OF 1977, 1991 AND 2001

4.2.2 DIGITAL AERIAL AND UAV DATASETS OF 2009 AND 2019

4.2.3 GNSS SURVEY FOR BLOCK GEOREFERENCING

4.3 METHODS

4.4 DISCUSSION

4.5 REFERENCES

5

Consectetuer adipiscing elit

LOREM IPSUM DOLOR SIT AMET, consectetuer adipiscing elit. Morbi commodo, ipsum sed pharetra gravida, orci magna rhoncus neque, id pulvinar odio lorem non turpis. Nullam sit amet enim. Suspendisse id velit vitae ligula volutpat condimentum. Aliquam erat volutpat. Sed quis velit. Nulla facilisi. Nulla libero. Vivamus pharetra posuere sapien. Nam consectetuer. Sed aliquam, nunc eget euismod ullamcorper, lectus nunc ullamcorper orci, fermentum bibendum enim nibh eget ipsum. Donec porttitor ligula eu dolor. Maecenas vitae nulla consequat libero cursus venenatis. Nam magna enim, accumsan eu, blandit sed, blandit a, eros.

6

Conclusion

Lorem ipsum dolor sit amet, consectetur adipiscing elit. Morbi commodo, ipsum sed pharetra gravida, orci magna rhoncus neque, id pulvinar odio lorem non turpis. Nullam sit amet enim. Suspendisse id velit vitae ligula volutpat condimentum. Aliquam erat volutpat. Sed quis velit. Nulla facilisi. Nulla libero. Vivamus pharetra posuere sapien. Nam consectetur. Sed aliquam, nunc eget euismod ullamcorper, lectus nunc ullamcorper orci, fermentum bibendum enim nibh eget ipsum. Donec porttitor ligula eu dolor. Maecenas vitae nulla consequat libero cursus venenatis. Nam magna enim, accumsan eu, blandit sed, blandit a, eros.

A

Some extra stuff

Lorem ipsum dolor sit amet, consectetur adipiscing elit. Morbi commodo, ipsum sed pharetra gravida, orci magna rhoncus neque, id pulvinar odio lorem non turpis. Nullam sit amet enim. Suspendisse id velit vitae ligula volutpat condimentum. Aliquam erat volutpat. Sed quis velit. Nulla facilisi. Nulla libero. Vivamus pharetra posuere sapien. Nam consectetur. Sed aliquam, nunc eget euismod ullamcorper, lectus nunc ullamcorper orci, fermentum bibendum enim nibh eget ipsum. Donec porttitor ligula eu dolor. Maecenas vitae nulla consequat libero cursus venenatis. Nam magna enim, accumsan eu, blandit sed, blandit a, eros.



THIS THESIS WAS TYPESET using L^AT_EX, originally developed by Leslie Lamport and based on Donald Knuth's T_EX. The body text is set in 11 point Egenolff-Berner Garamond, a revival of Claude Garamont's humanist typeface. The above illustration, "Science Experiment 02", was created by Ben Schlitter and released under CC BY-NC-ND 3.0. A template that can be used to format a PhD thesis with this look and feel has been released under the permissive MIT (x11) license, and can be found online at github.com/suchow/Dissertate or from its author, Jordan Suchow, at suchow@post.harvard.edu.